



# A LAGRANGIAN-EULERIAN SHELL-FLUID COUPLING ALGORITHM BASED ON LEVEL SETS

Fehmi Cirak\*

*Center for Advanced Computing Research  
California Institute of Technology  
Pasadena, CA 91125, U.S.A.*

Raúl Radovitzky<sup>†</sup>

*Department of Aeronautics and Astronautics  
Massachusetts Institute of Technology  
Cambridge, MA 02139, U.S.A.*

## Abstract

We propose a robust computational method for the coupled simulation of a compressible high-speed flow interacting with a highly flexible thin-shell structure. A standard Eulerian finite volume formulation on a fixed Cartesian mesh is used for the fluid, and a Lagrangian formulation based on subdivision finite elements on an unstructured mesh is used for the shell. The fluid-shell interface on the Cartesian mesh is tracked with level sets. The conservation laws at the interface are enforced by applying proper interface boundary conditions to the fluid and shell solvers at the beginning of each time step. The basic approach furnishes a general algorithm for explicit loose coupling of Lagrangian shell solvers with Cartesian grid-based Eulerian fluid solvers. The efficiency and robustness of the proposed approach is demonstrated with an airbag deployment simulation.

Key words: shell, fluid, shell-fluid interaction, finite elements, finite volumes, level sets

---

\*Corresponding author, cirak@cacr.caltech.edu, Fax: (626) 6283994

<sup>†</sup>rapa@mit.edu

# 1 Introduction

A large class of fluid-shell interaction problems requires a combined Lagrangian/Eulerian description of the governing dynamics. It is well known that Lagrangian formulations are inadequate for describing high-speed flows with significant vorticity and/or with large boundary deformations, since the computational mesh inevitably incurs deformation-induced distortions, which breaks the numerical method. This problem can be alleviated by recourse to continuous adaptive remeshing [23], but not cured in general, especially in three dimensions. Eulerian approaches with the field equations formulated in terms of spatial variables and fixed meshes are better suited for most fluid flows. By contrast, large deformations of shells are more adequately described in a Lagrangian framework. The principal advantage of the Lagrangian approach for shells lies in its ability to naturally track the evolution of material properties associated with the material points as well as in the treatment of boundary conditions at material surfaces such as free boundaries or fluid-shell interfaces. In contrast to Eulerian approaches, boundary conditions are enforced at material surfaces *ab initio* and require no special attention. For the aforementioned reasons we use in this work an Eulerian finite volume formulation for the fluid and a Lagrangian formulation based on subdivision finite elements for the shell.

A number of different basic strategies have been proposed for coupling the response of interacting solids and fluids. In the conventional Arbitrary-Lagrangian-Eulerian (ALE) approach [8, 28, 9, 25], the coupling of the fixed Eulerian and moving Lagrangian meshes is accomplished through an intermediate region in which the conforming mesh moves with a prescribed velocity. The specification of the mesh evolution in the transition region is crucial to the success of ALE methods, which unfortunately requires some a priori knowledge of the solution. In particular, for thin-shell structures with possibly very large deformations, the success of ALE methods is not always assured. The ALE method also requires the application of time consuming mesh updating techniques at each time step as the shell body undergoes large deformations.

Alternatively, interface capturing techniques for tracking moving interfaces in fluids do not require the conformity of the meshes at the interface (see e.g. [13, 12, 30, 11, 21, 3], among many others). In particular, sharp interface methods, such as the ghost fluid method [11] and the immersed boundary technique [21], have also been applied to Lagrangian-Eulerian solid-fluid coupling. In the ghost fluid method, the discontinuities in the flow field resulting from the interface are directly embedded in the solution through appropriately populated ghost cells. In contrast, the immersed boundary technique applies a set of singular forces to the flow equations in order to approximate the discontinuous character of the flow close to the interface.

Our approach has its origin in the ghost fluid method [11, 12] and is an extension of the Eulerian-Lagrangian coupling strategy for bulk solids with compressible energetic flows presented in references [2, 10, 17]. The dynamic deformations of the solid shell are formulated within a large-deformation Lagrangian finite element framework, and an Eulerian finite volume formulation is adopted for solving the compressible flow equations. The coupling between the Eulerian fluid solver and the Lagrangian shell solver is accomplished with a technique based on level sets. At each time step, the signed distance function (or level set) from the deformed shell surface is computed on the Eulerian grid by a demonstrably optimal algorithm proposed by Mauch [16]. The resulting implicit representation of the fluid-shell boundary in the deformed configuration is used to enforce the conservation laws at the boundary between the fluid and the solid.

The Kirchhoff-Love type thin-shell model, used in this work, takes the membrane as well as bending response of the surface into account and has been discretized with the subdivision finite elements [5, 6, 7]. The underlying kinematic assumptions allow for arbitrary large displacements as well as rotations of the shell. Using the subdivision shape functions, the displacement field within one finite element is interpolated through the displacements of the vertices attached to the element and the immediately adjacent vertices in the mesh. In the resulting discretization, the nodal displacements of the subdivision finite elements constitute the only unknowns of the shell problem. Importantly, in contrast to conventional shell elements with displacements and rotations as degrees of freedom, the coupling of subdivision shell elements with solid, or as in the present case fluid, volume elements does not lead to any ambiguities.

The outline of the paper is as follows. We first briefly describe the numerical formulations used for the shell and the fluid. Subsequently, the fluid-shell coupling algorithm is described in full detail. Finally, we present an example of application of the overall numerical method to the simulation of airbag deployment. This example demonstrates the feasibility and robustness of the proposed computational strategy in capturing the intricate features of the interaction between the flow and the shell.

## 2 Lagrangian Thin-Shell Solver

In the following, we give a brief summary of the shell model adopted and its discretization with subdivision finite elements. A detailed presentation of the used model and discretization technique can be found in references [5, 6]. A class of finite-deformation Kirchhoff-Love shell theories may be obtained from the kinematic ansatz:

$$\begin{aligned}\bar{\varphi}(\theta^1, \theta^2, \theta^3) &= \bar{\mathbf{x}}(\theta^1, \theta^2) + \theta^3 \bar{\mathbf{a}}_3(\theta^1, \theta^2) & \text{with} & \quad -\frac{\bar{t}}{2} \leq \theta^3 \leq \frac{\bar{t}}{2} \\ \varphi(\theta^1, \theta^2, \theta^3) &= \mathbf{x}(\theta^1, \theta^2) + \theta^3 \mathbf{a}_3(\theta^1, \theta^2) & \text{with} & \quad -\frac{\bar{t}}{2} \leq \theta^3 \leq \frac{\bar{t}}{2}\end{aligned}$$

where  $\bar{\varphi}(\theta^1, \theta^2, \theta^3)$  is the position vector of a material point associated with the convective coordinates  $\{\theta^1, \theta^2, \theta^3\}$  within the shell body in its undeformed configuration. Similarly,  $\varphi(\theta^1, \theta^2, \theta^3)$  is the position vector with respect to the deformed configuration of the shell. The functions  $\bar{\mathbf{x}}$  and  $\mathbf{x}$  furnish a parametric representation of the undeformed and deformed shell middle surfaces, respectively, and the pair  $\{\theta^1, \theta^2\}$  defines a system of surface curvilinear coordinates. The thickness of the undeformed shell is  $\bar{t}$  and the parameter  $\theta^3$  determines the position of a material point on the normal (director) to the undeformed middle surface. The unit normals to the undeformed and deformed shell middle surface are:

$$\bar{\mathbf{a}}_3 = \frac{\bar{\mathbf{x}}_{,1} \times \bar{\mathbf{x}}_{,2}}{\bar{j}} \quad \mathbf{a}_3 = \frac{\mathbf{x}_{,1} \times \mathbf{x}_{,2}}{j} \quad (1)$$

Here, the surface jacobian is defined with  $\bar{j} = |\bar{\mathbf{x}}_{,1} \times \bar{\mathbf{x}}_{,2}|$ , and the comma is used to denote partial differentiation. With the aid of these kinematic assumptions, the deformation gradient  $\mathbf{F}$  for the shell body may be expressed in the form [15]:

$$\mathbf{F} = \frac{\partial \varphi}{\partial \bar{\varphi}} = \frac{\partial \varphi}{\partial \theta^i} \otimes \frac{\partial \theta^i}{\partial \bar{\varphi}} \quad (2)$$

In this equation, the summation convention is assumed to be in force.

The potential energy of the shell body takes the form:

$$\Pi[\boldsymbol{\varphi}] = \int_{\bar{\Omega}} \int_{-\frac{\bar{t}}{2}}^{+\frac{\bar{t}}{2}} W(\mathbf{F}) \mu d\theta^3 d\bar{\Omega} + \Pi_{ext} = \Pi_{int} + \Pi_{ext} \quad (3)$$

where, for an hyperelastic material,  $W$  is the strain-energy density per unit undeformed volume,  $\Pi_{ext}$  is the potential of the externally applied forces, and  $\mu$  accounts for the curvature of the shell in the computation of the volume element [5]. The Kirchhoff-Love energy functional (3) of the thin-shell depends on the first and second order derivatives of the undeformed and deformed middle surface,  $\bar{\mathbf{x}}$  and  $\mathbf{x}$ . It is known from approximation theory that the convergence of the related conforming finite-element procedure requires smooth,  $C^1$ -continuous, shape functions. On unstructured meshes, it is not possible to ensure strict slope continuity across finite elements when the elements are endowed with purely local polynomial shape functions and the nodal degrees of freedom consist of displacements and slopes only. Inclusion of higher derivatives among the nodal variables lead to several well known difficulties, e.g. spurious oscillations in the solution, non-physical higher order derivatives at the boundary vertices, or complex schemes for nonsingular parameterization of the derivatives for large rotations. These difficulties can be avoided by using *nonlocal* subdivision shape functions for the discretization of Kirchhoff-Love type shell theories on unstructured meshes.

In the subdivision scheme based finite element method, the discretized shell surface is entirely determined by the vertex positions of the triangulation, or *control mesh*. This results in a particularly simple discretization of the undeformed and deformed shell surfaces within one finite element [5]:

$$\bar{\mathbf{x}}_h = \sum_{I=1}^{NP} N^I \bar{\mathbf{x}}_I \quad \mathbf{x}_h = \sum_{I=1}^{NP} N^I \mathbf{x}_I \quad (4)$$

where  $\bar{\mathbf{x}}_I$  and  $\mathbf{x}_I$  are the vertex coordinates, and  $NP$  is the number of the vertices in the one neighborhood of the element, Figure 1. The subdivision method guarantees that all such element patches exactly match at their boundaries at least in  $C^1$  sense. Introducing the discretization into (3) and using the principle of minimum potential energy yields a discrete system of nonlinear algebraic equations for the equilibrium configurations:

$$\mathbf{f}_h^{int}(\mathbf{x}_h) = \mathbf{f}_h^{ext}(\mathbf{x}_h) \quad (5)$$

where  $\mathbf{f}_h^{int}(\mathbf{x}_h)$  is the internal force vector and  $\mathbf{f}_h^{ext}(\mathbf{x}_h)$  is the external force vector. If inertia effects are important, as in shell-fluid interaction problems, the Hamilton's principle of stationary action leads to a semi-discrete system of equations:

$$\mathbf{M}_h \ddot{\mathbf{x}}_h + \mathbf{f}_h^{int}(\mathbf{x}_h) = \mathbf{f}_h^{ext}(\mathbf{x}_h, t) \quad (6)$$

where  $\mathbf{M}_h$  is the mass matrix and  $\ddot{\mathbf{x}}_h$  is the acceleration vector. In our shell-fluid coupling framework, the external force vector  $\mathbf{f}_h^{ext}(\mathbf{x}_h, t)$  includes, among others, the pressure loading exerted from the fluid on to the shell (see section 4).

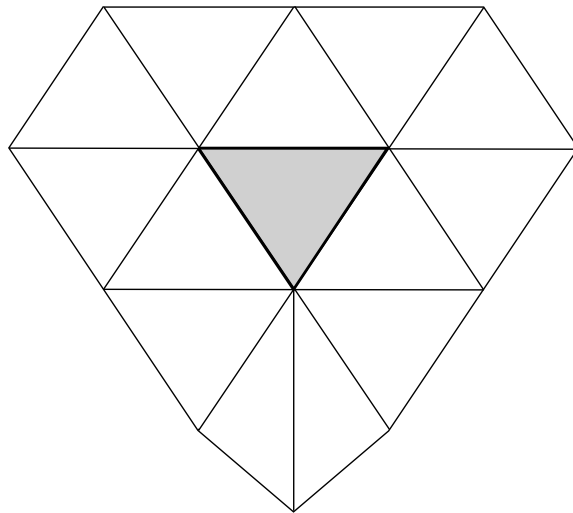


Figure 1: Triangular element and its thirteen control nodes.

The semi-discrete equations of motion (6) are integrated in time with the explicit predictor-corrector type Newmark algorithm:

$$\mathbf{x}_{n+1} = \mathbf{x}_n + \Delta t \dot{\mathbf{x}}_n + \frac{1}{2} \Delta t^2 \ddot{\mathbf{x}}_n \quad (7)$$

$$\dot{\mathbf{x}}_{pre} = (1 - \gamma_{Newmark}) \Delta t \ddot{\mathbf{x}}_n + \dot{\mathbf{x}}_n \quad (8)$$

in which  $\gamma_{Newmark}$  is the Newmark damping parameter (with  $0.5 \leq \gamma_{Newmark} \leq 1$ ) and  $\dot{\mathbf{x}}_{pre}$  is the predictor velocity vector. The final velocities follow from:

$$\ddot{\mathbf{x}}_{n+1} = \mathbf{M}^{-1}(\mathbf{f}_n^{ext} - \mathbf{f}_n^{int}(\mathbf{x}_{n+1})) \quad (9)$$

$$\dot{\mathbf{x}}_{n+1} = \dot{\mathbf{x}}_{pre} + \gamma_{Newmark} \Delta t \ddot{\mathbf{x}}_{n+1} \quad (10)$$

### 3 Eulerian Compressible Fluid Solver

In this section, we summarize the details of the employed fluid solver for the inviscid compressible flow. The set of governing Euler equations can be written as:

$$\begin{aligned} \frac{\partial \rho}{\partial t} + \nabla \cdot (\rho \mathbf{u}) &= 0 \\ \frac{\partial}{\partial t} (\rho \mathbf{u}) + \nabla \cdot (\rho \mathbf{u} \otimes \mathbf{u} + \mathbf{I} p) &= 0 \\ \frac{\partial}{\partial t} (\rho E) + \nabla \cdot \left[ \rho \mathbf{u} \left( E + \frac{p}{\rho} \right) \right] &= 0 \end{aligned} \quad (11)$$

where  $\rho$  is the density,  $\mathbf{u}$  is the velocity vector,  $p$  is the pressure,  $E = e + \frac{1}{2} \|\mathbf{u}\|^2$  is the specific total energy, and  $e$  is the specific internal energy. The above equations are closed by an additional equation of state. In the case of a perfect gas, the equation of state takes the form:

$$e = \frac{p}{(\gamma - 1)\rho} \quad (12)$$

in which  $\gamma$  is the constant specific heat ratio.

The Euler equations may be written in conservative form:

$$\mathbf{U}_{,t} + \nabla \cdot \mathbf{F} = \mathbf{0} \quad (13)$$

where  $\mathbf{U}$  is the vector of unknowns and  $\mathbf{F}$  is the flux vector. In our framework, the fluid domain is discretized with a fixed Cartesian grid with a possibly non-uniform cell size. Using a dimensional splitting approach, the three dimensional problem (13) is reduced to a sequence of one-dimensional problems along each coordinate direction. The resulting one-dimensional problems are discretized with a finite volume approach so that the first order correct discrete solution follows from:

$$\mathbf{U}_i^{n+1} = \mathbf{U}_i^n + \frac{\Delta t}{h} (\mathbf{F}_{i-1/2}^n - \mathbf{F}_{i+1/2}^n) \quad (14)$$

where  $\mathbf{U}_i^{n+1}$  is the average of the cell  $i$  at time step  $n + 1$ ,  $\Delta t$  is the time step size,  $h$  is the cell size, and  $\mathbf{F}_{i-1/2}^n$  and  $\mathbf{F}_{i+1/2}^n$  are the fluxes through the left and right cell boundary. Taking the hyperbolic character of the compressible Euler equations into account, a particularly efficient method for approximating the interface fluxes in (14) consists of solving local Riemann problems at each cell interface. For real gases, the local Riemann problems may be solved using Roe's approximate solver [24]. Although the sketched discretization scheme is first order in space as well as in time, it serves as a starting point for many higher order schemes.

In the present framework, the spatially-discretized equations are integrated in time with the second-order Runge-Kutta algorithm. Second order accuracy is achieved via linear reconstruction with Van Leer type slope limiting applied to projections in characteristic state space [26, 14]. A review of the various schemes for approximating the fluxes and their extension to higher order schemes may be found in standard text books [14]. For more details of the particular formulation employed and its parallel implementation including adaptive mesh refinement capability we refer to reference [1].

## 4 Eulerian-Lagrangian Fluid-Shell Coupling

A critical aspect of any Eulerian-Lagrangian fluid-shell coupling strategy is to formulate a theoretically sound and, at the same time, computationally effective means to algorithmically couple the fluid and shell solvers. For the explicit dynamics case, one approach is to loosely couple the two solvers by applying appropriate interface boundary conditions at the beginning of each time step. The interface boundary conditions follow from explicitly enforcing the

- continuity of the normal velocity
- continuity of the pressure

at the interface. In the fluid solver, normal velocity continuity and free-tangential-flow (slip) boundary conditions, required for the inviscid Euler model, may be enforced through a narrow band of so-called ghost cells outside the physical fluid domain, Figure 2. The field variables in the ghost cells, namely the fluid velocity, pressure, and density, are chosen in dependence of the solution within the physical domain and the shell velocity.

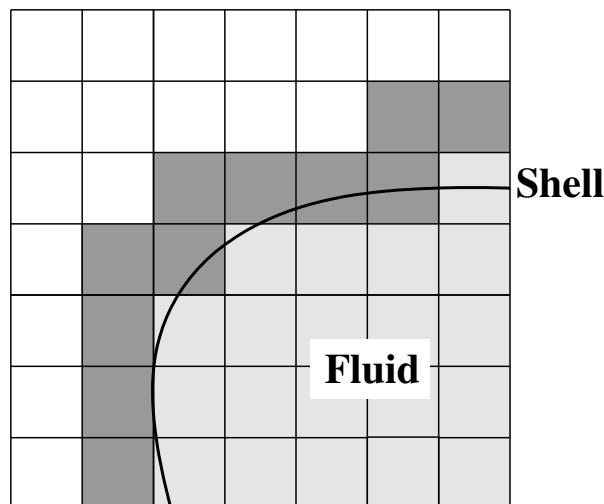


Figure 2: Identification of the fluid and the ghost cells given the instant location of the shell.

First, the ghost cells are populated by extrapolating the velocity, pressure, and density cell averages from adjacent active fluid cells. Various approaches for the extrapolation are conceivable, such as constant extrapolation from the closest point on the interface, extrapolation with the fast extension methods [29], or propagation with the eikonal equation [2], as in our framework,

$$\frac{\partial \alpha}{\partial t} + \mathbf{n} \cdot \nabla \alpha = 0 \quad (15)$$

where  $\alpha$  is the variable to be extrapolated and  $\mathbf{n}$  is the interface normal. Subsequently, the ghost cell velocities are modified so that the relative fluid velocity normal to the interface is zero:

$$\mathbf{u}_{Fluid} = [(2\mathbf{u}_{Shell} - \tilde{\mathbf{u}}_{Fluid}) \cdot \mathbf{n}] \mathbf{n} + [\tilde{\mathbf{u}}_{Fluid} - (\tilde{\mathbf{u}}_{Fluid} \cdot \mathbf{n}) \mathbf{n}] \quad (16)$$

where  $\tilde{\mathbf{u}}_{Fluid}$  is the fluid velocity extrapolated from the active fluid cells and  $\mathbf{u}_{Shell}$  is the shell velocity extrapolated from the shell middle surface. Note that for the case of zero shell velocity and spatially matching interface shell and fluid nodes equation (16) enforces a reflecting type boundary condition at the interface. The velocity component normal to the interface  $(\tilde{\mathbf{u}}_{Fluid} \cdot \mathbf{n}) \mathbf{n}$  is simply reflected with  $-(\tilde{\mathbf{u}}_{Fluid} \cdot \mathbf{n}) \mathbf{n}$  and the tangential velocity component  $(\tilde{\mathbf{u}}_{Fluid} - \tilde{\mathbf{u}}_{Fluid} \cdot \mathbf{n}) \mathbf{n}$  is not constrained. After setting the velocity values in the ghost cells at the beginning of each time step, the standard fluid solver is applied to the entire Cartesian mesh without any modifications.

In order to enforce the pressure continuity at the shell-fluid interface, the pressure on the shell surface is interpolated from the adjacent real fluid cells at the beginning of each time step. The interpolated pressure is applied as a traction boundary condition on the shell finite element mesh, which in effect accomplishes the momentum transfer from the fluid to the shell.

A key element for the success of the proposed coupling strategy is the availability of a fast and scalable algorithm for determining the shell position on the Cartesian fluid mesh at each time step. In our framework, the location of the shell relative to each fluid cell is obtained by

recourse to a level set function. The level set function  $\phi(\mathbf{x})$  at a point  $\mathbf{x}$  is defined as the signed distance to the shell middle surface:

$$\phi(\mathbf{x}) \begin{cases} < 0 & \text{ghost fluid domain} \\ = 0 & \text{shell middle surface} \\ > 0 & \text{physical fluid domain} \end{cases} \quad (17)$$

Further, the normal to the interface may be computed by evaluating the expression

$$\mathbf{n} = \frac{\nabla\phi}{\|\nabla\phi\|} \quad (18)$$

with central differencing. The signed distance function can be most efficiently computed with the linear time algorithm developed by Mauch [16]. Using Mauch's algorithm, we compute at the beginning of each time step the signed distance of the fluid cells to the deformed shell mesh without using any information about the prior position or velocity of the interface. Alternatively, it is possible to dynamically update the level set information by propagating the interface with the known interface velocities, e.g., as proposed in [27].

For the signed distance function computation and coupling purposes, the smooth deformed shell surface is approximated by the control mesh. Importantly, the control mesh positions and velocities are for the approximating subdivision schemes different from the positions and velocities of the represented limit surface. However, for a given control mesh the limit positions and velocities can easily be computed with compact limit masks, see e.g. [6]. We use the limit positions and velocities as the input for the coupling algorithm.

In summary, the introduced coupling strategy leads to a robust and scalable method for the treatment of high-speed flows interacting with highly-deformable solids. The stable time step size for the shell or fluid solvers is not negatively influenced by the coupling procedure. The coupling algorithm's overall computational complexity is determined by the level set computation and is of order  $O(m + n)$ , where  $m$  is the number of grid points in the subset of the fluid grid where the level set is required and  $n$  is the number of elements in the shell mesh.

## 5 Example

We consider the simulation of airbag deployment for demonstrating the feasibility and power of the developed method in computing the complex interactions of high speed flows with highly-deformable thin-shell structures.

The simulation corresponds to an initially-flat airbag made of an elastic fabric with a Young's modulus of  $E = 6.0 \cdot 10^9 Pa$ , Poisson's ratio of  $\nu = 0.3$ , and mass density of  $\rho = 1000.0 \frac{kg}{m^3}$ , Figure 3. The thickness of the airbag is  $7.3 \cdot 10^{-4}m$  and the diameter in its flat initial configuration is  $D = 0.74m$ . The discretization of the airbag consists of 10176 subdivision thin-shell elements and 5101 vertices. Due to the extreme thinness, it may appear justified to neglect the bending resistance and to idealize the airbag fabric as a membrane. However, the bending energy plays a crucial role in determining the size and folding patterns of the shell [5, 22, 20, 4] and therefore can be expected to have an important influence on the fluid flow.

The gas enters the airbag with a pressure of  $p = 12.0atm$ , mass density of  $\rho = 16.0 \frac{kg}{m^3}$ , and vertical velocity of  $u_z = 73.0 \frac{m}{s}$ . The initial properties of the gas are:  $p = 1.0atm$ ,  $\rho = 13.0 \frac{kg}{m^3}$ ,

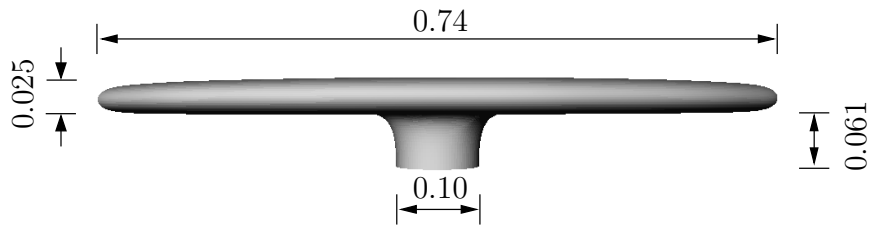


Figure 3: Airbag geometry.

and  $\gamma = 1.4$ . The expanding gas generates a weak shock wave that propagates inside the airbag and interacts with the airbag walls. The inlet conditions of the gas are kept constant until  $9.71ms$  and later changed to reflecting type boundary conditions. The fluid domain of  $0.86m \times 0.86m \times 0.49m$  is discretized with  $48 \times 48 \times 62$  fluid cells. For the fluid-shell interaction only the fluid inside the airbag volume is considered.

Figures 4 and 5 show a sequence of snapshots of the simulation. The deformed airbag meshes are shown on Figure 4 and the shell limit surface with the density isocontours of the enclosed fluid in Figure 5. The portions of the fluid grid that are external to the airbag have been left out for visual clarity by making use of the level set function. Important features of the mechanics of the airbag deployment process can be observed in these figures, including the high-frequency wrinkling modes of the airbag fabric and the shock reflections of the gas on the deforming airbag walls. The computed maximum displacement of the airbag fabric is  $0.48m$  and the total simulation time  $32.5ms$ , Figure 6. The ability of the presented method to capture these complex features of the coupled interaction between the flow and the highly flexible airbag fabric is particularly noteworthy.

The simulations were performed using 58 Intel Pentium III® processors on a Beowulf cluster with a one *Gbps* fast Ethernet switch. The computation time for the whole simulation was approximately 15 hours.

## 6 Conclusions

We have developed a robust and efficient numerical approach for the simulation of compressible flows interacting with highly-deformable thin-shells. The method furnishes an effective means of coupling Cartesian mesh based Eulerian fluid solvers and Lagrangian subdivision shells, thus exploiting the strength of these particular formulations. The versatility and excellent robustness of the approach has been demonstrated with a simulation of an airbag deployment process. The proposed coupling approach enables the modeling of the fluid, shell, and their interaction in full detail with an equivalent level of fidelity without any oversimplifying assumptions, as is common in many fluid-solid interaction methods.

In closing, a number of possible extensions of the theory are worth mentioning. Firstly, the presented coupling algorithm is not conservative and only first order accurate. In particular, the conservation or higher order accuracy of the discrete mass and momenta at the interface is very desirable for many shell fluid interaction problems. Indeed, there are conserving or higher order Eulerian front tracking schemes available[19, 18], which might be extendable to shell fluid in-

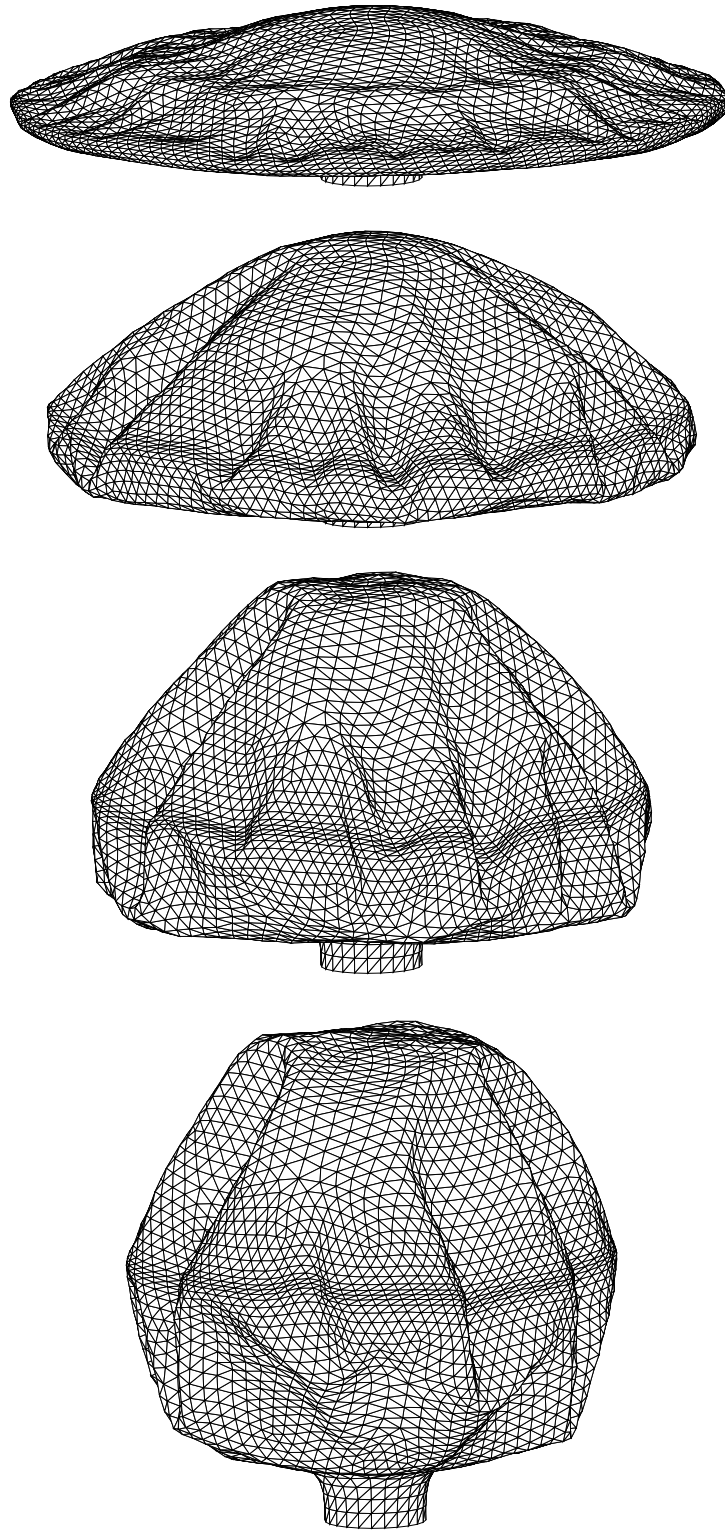


Figure 4: Deformed control meshes at step 2500 (4.25 *ms*), 5000 (8.16 *ms*), 7500 (12.13 *ms*), and 10000 (18.02 *ms*).

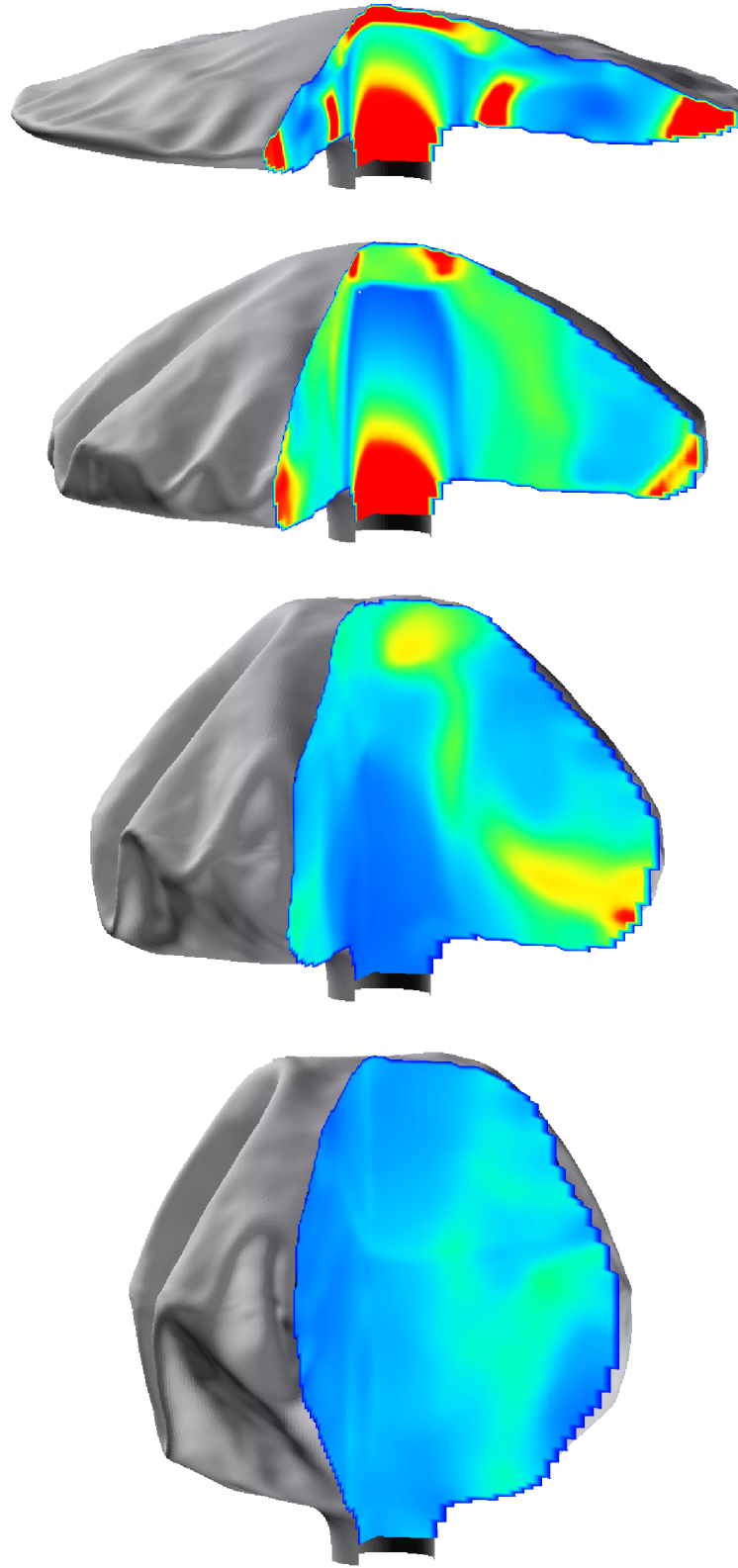


Figure 5: Deformed limit surfaces and density iso-contours of the enclosed fluid at step 2500 ( $4.25\text{ ms}$ ), 5000 ( $8.16\text{ ms}$ ), 7500 ( $12.13\text{ ms}$ ), and 10000 ( $18.02\text{ ms}$ ).

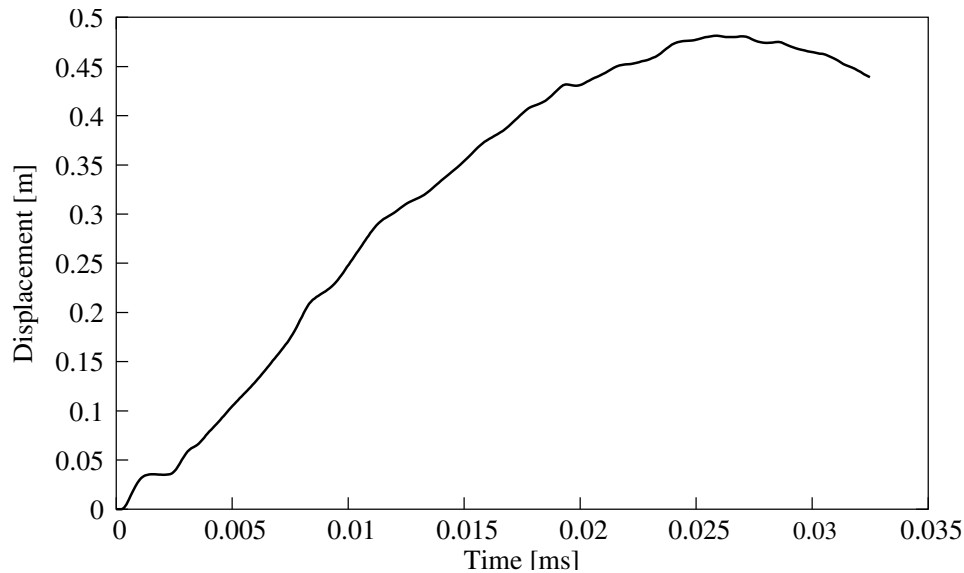


Figure 6: Maximum vertical displacement history.

teraction problems. For problems involving permeable membranes, such as the airbag inflation, there is also a need for the controlled dissipation of the mass and momenta at the interface due to the permeability of the woven membrane. Finally, a large class of shell structures, such as plates, do not have a uniquely identifiable inside or outside and in that context, the notion of a signed distance is meaningless. For such problems, a similar coupling strategy based on the distance and the normal information of the oriented shell surface appears to be feasible.

## Acknowledgments

The partial support of DoE through Caltech's ASCI Center is gratefully acknowledged (DOE W-7405-ENG-48, B523297). We are grateful to the other members of the Virtual Test Facility software development team: Michael Aivazis, Julian Cummings, Dan Meiron, and Ravi Samtaney for their contributions to the VTF.

## References

- [1] M. Aivazis, B. Goddard, D. Meiron, M. Ortiz, J.C.T. Pool, and J. Shepherd. ASCI Alliance Center for the Simulation of Dynamic Response of Materials, FY00 Annual Report. URL: <http://www.cacr.caltech.edu/ASAP/publications/annualreps.html>, 2000.
- [2] M. Arienti, P. Hung, and J. Morano, E.and Shepherd. A level set approach to eulerian-lagrangian coupling. *J. Comput. Phys.*, 185:213–251, 2003.
- [3] J. Chessa and T. Belytschko. An extended finite element method for two-phase fluids. *Transactions of the ASME*, 70:10–17, 2003.

- [4] F. Cirak, J.E. Cisternas, A.M. Cuitino, G. Ertl, P. Holmes, I.G. Kevrekidis, M. Ortiz, H.H. Rotermund, M. Schunack, and J. Wolff. Oscillatory thermomechanical instability of an ultrathin catalyst. *Science*, 300:1932–1936, 2003.
- [5] F. Cirak and M. Ortiz. Fully  $c^1$ -conforming subdivision elements for finite deformation thin-shell analysis. *Internat. J. Numer. Methods Engrg.*, 51:813–833, 2001.
- [6] F. Cirak, M. Ortiz, and P. Schröder. Subdivision surfaces: A new paradigm for thin-shell finite-element analysis. *Internat. J. Numer. Methods Engrg.*, 47(12):2039–2072, 2000.
- [7] F. Cirak, M.J. Scott, E.K. Antonsson, M. Ortiz, and P. Schröder. Integrated modeling, finite-element analysis, and engineering design for thin-shell structure using subdivision. *Computer-Aided Design*, 34:137–148, 2002.
- [8] J. Donea, S. Guiliani, and J.P. Halleux. An arbitrary lagrangian-eulerian finite element method for transient fluid-structure interactions. *Computer Methods in Applied Mechanics and Engineering*, 33:689–723, 1982.
- [9] C. Farhat, M. Lesoinne, and LeTallec P. Load and motion transfer algorithms for fluid/structure interaction problems with non-matching discrete interfaces: Momentum and energy conservation, optimal discretization and application to aeroelasticity. *Computer Methods in Applied Mechanics and Engineering*, 157:95–114, 1998.
- [10] R.P. Fedkiw. Coupling an eulerian fluid calculation to a lagrangian solid calculation with the ghost fluid method. *J. Comput. Physics*, 175:200–224, 2002.
- [11] R.P. Fedkiw, T. Aslam, B. Merriman, and S. Osher. A non-oscillatory eulerian approach to interfaces in multimaterial flows (the ghost fluid method). *J. Comput. Physics*, 152:457–492, 1999.
- [12] J. Glimm and D. Marchesin. A numerical method for two phase flow with an unstable interface. *Journal of Computational Physics*, 39:179–200, 1981.
- [13] C.W. Hirt and B.D. Nichols. Volume of fluid (vof) method for the dynamics of free boundaries. *Journal of Computational Physics*, 39:382–408, 1981.
- [14] R.J. LeVeque. *Finite Volume Methods for Hyperbolic Problems*. Cambridge University Press, 2002.
- [15] J. E. Marsden and T. J. R. Hughes. *Mathematical foundations of elasticity*. Prentice-Hall, Englewood Cliffs, N.J., 1983.
- [16] S. Mauch. A fast algorithm for computing the closest point and distance transform. *Preprint*, <http://www.acm.caltech.edu/~seanm/software/cpt/cpt.html>, 2001.
- [17] D. Meiron, R. Radovitzky, and R. Samtaney. The virtual test facility: An environment for simulating the nonlinear dynamic response of solids under shock and detonation wave loading. In *Proceedings of the Sixth U.S. National Congress on Computational Mechanics*, Dearborn, MI, 2001. U.S. Association for Computational Mechanics.

- [18] D. Modiano and P. Colella. A higher-order embedded boundary method for time-dependent simulation of hyperbolic conservation laws. Technical Report LBNL-45239, Lawrence Berkeley National Laboratory, 2000.
- [19] D. Nguyen, F. Gibou, and Fedkiw R. A fully conservative ghost fluid method & stiff detonation waves. In *12th Int. Detonation Symposium*, San Diego, CA, 2002.
- [20] M. Ortiz and G. Gioia. The morphology and folding patterns of buckling-driven thin-film blisters. *Journal of the Mechanics and Physics of Solids*, 42:531–559, 1994.
- [21] C.S Peskin. Numerical-analysis of blood-flow in heart. *Journal of Computational Physics*, 25:220–252, 1977.
- [22] A.C. Pipkin. The relaxed energy density for isotropic elastic membranes. *IMA Journal of Mathematics*, 36:85–99, 1986.
- [23] R. Radovitzky and M. Ortiz. Lagrangian finite element analysis of newtonian fluid flows. *International Journal For Numerical Methods In Engineering*, 43(4):607–617, 1998.
- [24] P.L. Roe. Approximate riemann solvers, parameter vectors, and difference schemes. *Journal of Computational Physics*, 43:357–372, 1981.
- [25] S. Rugonyi and K.J. Bathe. On finite element analysis of fluid flows fully coupled with structural interactions. *CMES - Computer Modeling in Engineering & Sciences*, 2:195–212, 2001.
- [26] R. Samtaney and D. I. Meiron. Hypervelocity Richtmyer-Meshkov instability. *Physics of Fluids*, 9(6):1783–1803, 1997.
- [27] J.A. Sethian and P. Smereka. Level set methods for fluid interfaces. *Annual Review of Fluid Mechanics*, 33:341–372, 2003.
- [28] K. Stein, R. Benney, T. Tezduyar, and J. Potvin. Fluid-structure interactions of a cross parachute: Numerical simulation. *Computer Methods in Applied Mechanics and Engineering*, 191:673–687, 2001.
- [29] J.N. Tsitsiklis. Efficient algorithms for globally optimal trajectories. *IEEE Transactions on Automatic Control*, 40:1528–1538, 1995.
- [30] T. Yabe, F. Xiao, and T. Utsumi. The constrained interpolation profile method for multi-phase analysis. *Journal of Computational Physics*, 169:556–593, 2001.